J. Fluid Mech. (1980), *vol.* 97, *part* 3, *pp.* 513–530
Printed in Great Britain

Coupled interactions of shock-wave structure with laminar boundary layers in ionizing-argon flows

By W. S. LIU†, K. TAKAYAMA‡ AND I. I. GLASS
Institute for Aerospace Studies, University of Toronto, Ontario, Canada

(Received 9 March 1979)

Analyses are made of the mutual interactions between shock structure and the side-wall laminar boundary layer and their effects on the quasi-steady flat-plate laminar boundary layer in ionizing-argon shock-tube flows. The mutual interactions are studied using effective quasi-one-dimensional equations derived from an area-averaged-flow concept in a finite-area shock tube. The effects of mass, momentum and energy non-uniformities and the wall dissipations in the ionization and relaxation regions on the argon shock structure are discussed. The new results obtained for shock structure, shock-tube laminar side-wall and quasi-steady flat-plate boundary-layer flows are compared with dual-wavelength interferometric data obtained from the UTIAS 10×18 cm Hypervelocity Shock Tube. It is shown that the difference between the results obtained from the present method and those obtained by Enomoto based on Mirels' perfect-gas boundary-layer solutions are significant for lower shock Mach numbers ($M_s \sim 13$) where the relaxation lengths are large (~ 10 cm). In general, the present results agree better with our experimental data than our previous results for uncoupled ionizing flows.

1. Introduction

In our previous analyses of ionizing shock-wave structures (Glass, Liu & Tang 1977; Glass & Liu 1978) and the ionizing boundary-layer flows induced by a strong shock wave (Liu, Whitten & Glass 1978; Liu & Glass 1979), the coupled effects between inviscid and viscous flows in a shock tube were neglected. As shown by Glass & Patterson (1955) and Mirels (1966), the flow between the shock wave and the contact surface in an actual shock tube is non-uniform owing to the growth of the shock-tube side-wall boundary layer. The gross features of shock-wave structure in an ionizing gas are affected by the side-wall boundary layer. Consequently, the induced ionizing boundary layers on a flat plate in the so-called quasi-uniform flow are affected by these mutual interactions. This non-uniformity has to be considered when interpreting shock-tube data (Brabbs & Belles 1971).

The important effects of the growth of the side-wall boundary layer on the free-stream flow are the induced wall shearing stress, heat transfers and the consequent non-uniformities in the flow. In order to take into account the flow non-uniformities in a shock-tube, Mirels (1963, 1964, 1966) obtained correlation formulae for a perfect gas,

† Present address: Atomic Energy of Canada Research Company, Pinawa, Manitoba, Canada R0E 1L0.
‡ Visiting Associate Professor, Tohoku University, Sendai, Japan.

0022-1120/80/4417-8620 $02.00

which are often used by many researchers in gasdynamics. These relations are based on similarity solutions of the boundary-layer equations treating the boundary layer as an aerodynamic sink. Local-similarity assumptions cannot be applied to those cases where the variations of the free-stream-flow quantities are important and cannot be neglected. As shown by Liu and co-workers (1978, 1979) the similarity assumption is not valid for the electron-temperature and electron number-density profiles for the side-wall boundary-layer flow where ionizing non-equilibrium phenomena occur in the free-stream flow behind the shock front and the variations of the free-stream conditions for the side-wall boundary layer are significant. Also, only mass conservation was considered by Mirels in the study of flow non-uniformity, and the effects of the side-wall boundary layer on the free-stream momentum and energy equations were neglected. The validity of Mirels' correlation formulae cease to apply to an ionizing-gas flow, although they were used by Enomoto (1973), McLaren & Hobson (1968) and Brabbs & Belles (1971) in their studies of shock structure in an ionizing gas. Enomoto studied the side-wall boundary-layer effects on ionizing shock structure in argon. He applied Mirels' (1966) perfect-gas-correlation formulae for flow non-uniformity of the mass mixture. Flow non-uniformities in the momentum and energy equations were entirely neglected without giving any reasons. Nevertheless, he found the important physical result that the relaxation length is significantly reduced in tubes of decreasing cross-sectional area owing to the side-wall boundary-layer growth.

The side-wall boundary-layer growth generates both compression and rarefaction characteristics. However, the net effect is that of a rarefaction wave which attenuates the shock front (Trimpi & Cohen 1955). Flow uniformity in ionizing gases in the relaxation regions induced by incident and reflected shock waves is still far from being completely understood. In principle, an analysis can be made by taking account of the interaction between the boundary-layer growth and the development of a two- or three-dimensional inviscid-flow model. For example, Hubbard & de Boer (1969) studied two-dimensional flow non-uniformities in a perfect gas based on the assumption that the boundary-layer parameters do not change very much in the region where two-dimensional effects are of importance. They showed that the flow in the inviscid region is nearly one-dimensional at a distance from the shock front greater than the shock-tube radius. In the usual one-dimensional model, the boundary layer is assumed thin compared to the shock-tube radius and is replaced by a sink distribution. The inviscid core is assumed to be quasi-one-dimensional in the sense that flow variations are assumed to occur only in the streamwise direction. In the present analysis, the inviscid core field is assumed to be effectively one-dimensional by using an area-averaging process, instead of treating the boundary layer as a sink.

The purpose of this work is to extend our previous studies of shock-wave structure and boundary-layer flows in ionizing argon by including the mutual interactions between the inviscid free-stream and viscous side-wall boundary-layer flows. The mutual interactions are studied based on the effective one-dimensional-flow equations derived from the flow area-averaged concept, where the flow non-uniformities in the free-stream mass, momentum and energy equations and in the wall dissipation terms are considered. A finite-difference scheme is applied to the ionizing boundary-layer equations. An examination follows of the role of the side-wall boundary-layer growth on the behaviour of the shock-structure ionization and radiation-cooling regions.

The results of the quasi-steady flat-plate and the side-wall boundary-layer flows

induced by a strong shock wave in a finite area shock tube are re-examined and compared with our dual-wavelength interferometric boundary-layer data obtained from the UTIAS 10×18 cm Hypervelocity Shock Tube. It is shown that the difference between the results obtained from the present method and the simplified Mirels' one-dimensional equations are even more significant at lower shock Mach number where the relaxation lengths are larger. In general, the present analysis gives much better agreement with our experimental data by taking into account the mutual interactions between the inviscid and viscous flows.

2. Theoretical considerations

Two methods have been widely applied in obtaining the effective quasi-one-dimensional-flow equations in gas mixtures: (1) control-volume method and (2) flow area-averaged method. In the former, the integral form of the conservation law is applied to the mixture control volume. The effective equations are then obtained by introducing definitions of area-averaged properties and limiting the length of the control volume to zero. In the latter, local instantaneous conservation equations are obtained from the law of conservation and the effective quasi-one-dimensional-flow equations are obtained by applying an area average on the local instantaneous conservation equations. Identical results are obtained from both methods for a homogeneous gas-mixture flow.

In this work, the effective quasi-one-dimensional-flow equations for an ionized gas in a shock tube are directly obtained by applying the flow area-average on the local instantaneous macroscopic-balance equations. The governing equations for a steady one-dimensional flow for an ionizing gas are (Takayama & Liu 1979)

$$\frac{d}{dx}\rho u(A-\delta^* L) = 0, \tag{1}$$

$$\frac{d}{dx}\rho u^2(A-\delta_m L) + A\frac{dp}{dx} = -L\left(\mu\frac{\partial u}{\partial y}\right)_w, \tag{2}$$

$$\frac{5}{2}\frac{d}{dx}pu(A-\delta_u L) + RT_I\frac{d}{dx}\rho u\alpha(A-\delta_\alpha L) + \frac{1}{2}\frac{d}{dx}\rho u^3(A-\delta_e L)$$
$$= -Q_R(A-\delta_R L) - L\left(\mu u\frac{\partial u}{\partial y}\right)_w + L(q_d+q_c)_w, \tag{3}$$

$$\frac{d}{dx}\rho u\alpha(A-\delta_\alpha L) = m_a\dot{n}_e(A-\delta_{\dot{n}_e}L) - L\left(\rho D_{\mathrm{am}}\frac{\partial\alpha}{\partial y}\right)_w, \tag{4}$$

$$\frac{3}{2}\frac{d}{dx}\rho u\alpha RT_e(A-\delta_{T_e}L) + \rho\alpha RT_e(A-\delta_{n_e}L)\frac{d}{dx}u(A-\delta_u L)$$
$$= -L(q_{ce}+q_{de})_w + (Q_{\mathrm{el}}+Q_{\mathrm{inel}})(A-\delta_Q L). \tag{5}$$

Here ρ is the plasma density, u the velocity, A the shock-tube cross-section area, L the shock-tube-perimeter length, p the plasma pressure; μ the plasma-viscosity coefficient, T the temperature, α the degree of ionization, Q_R the radiation energy loss, q_c and q_d the plasma-heat conduction and diffusive-energy fluxes, respectively, n_e the electron-production rate, D_{am} the ambipolar-diffusion coefficient, R the plasma gas constant,

Q_{el} and Q_{inel} are the elastic and inelastic energy-transfer rates to free electrons, respectively; subscripts w, I, e denote wall, ionization and electrons, respectively. In the derivation of (1)–(5) the second-order terms in the momentum and energy equations are negligible compared with the wall-dissipation terms. The effect of electron thermal conduction on the relaxation profiles has been investigated by Kamimoto, Teshima & Nishimura (1972). They concluded that the contribution of the electron thermal conduction terms on the relaxation profiles is insignificant and can be neglected.

The following boundary-layer thicknesses are defined:

$$\left.\begin{aligned}
\delta^* &= \int(1-\rho u/\rho_\delta u_\delta)\,dy;\\
\delta_m &= \int(1-\rho u^2/\rho_\delta u_\delta^2)\,dy;\\
\delta_u &= \int(1-u/u_\delta)\,dy;\\
\delta_\alpha &= \int(1-\rho u\alpha/\rho_\delta u_\delta \alpha_\delta)\,dy;\\
\delta_e &= \int(1-\rho u^3/\rho_\delta u_\delta^3)\,dy;\\
\delta_R &= \int(1-Q_R/Q_{R\delta})\,dy;\\
\delta_{\dot{n}_e} &= \int(1-\dot{n}_e/\dot{n}_{e\delta})\,dy;\\
\delta_{T_e} &= \int(1-\rho u\alpha T_e/\rho_\delta u_\delta \alpha_\delta T_{e\delta})\,dy;\\
\delta_{n_e} &= \int(1-n_e/n_{e\delta})\,dy;\\
\delta_Q &= \int[1-(Q_{\mathrm{el}}+Q_{\mathrm{inel}})/(Q_{\mathrm{el},\delta}+Q_{\mathrm{inel},\delta})]\,dy.
\end{aligned}\right\} \tag{6}$$

The subscript δ denotes the edge of the boundary layer. It should be noted that δ^*, δ_m, δ_u and δ_e are negative and δ_R, $\delta_{\dot{n}_e}$, δ_{n_e} and δ_Q are positive. The signs of δ_α and δ_{T_e} depend on the flow profiles inside the boundary layer.

The governing equations for a quasi-one-dimensional ionizing-gas flow used by Enomoto (1973) based on Mirels' method can be obtained from equations (1)–(5) by letting all the δ's, except the displacement thickness δ^*, equal zero and neglecting all dissipation terms. According to the correlation formulae proposed by Mirels (1966) based on similarity assumptions in the boundary-layer solution, Enomoto used the following equation:

$$A-\delta^* L = A\,[1-(x/l_m)^N]^{-1}, \tag{7}$$

where $N = 0{\cdot}5$ for a laminar boundary-layer flow and l_m is calculated from the formulas given by Mirels (1964).

Equations (1)–(5) were solved by Glass and co-workers (1977, 1978) for shock-wave structures of ionizing argon and krypton without taking into account the flow non-uniformities and the dissipation terms. The results were compared with our interferometric data in some detail. The δ's and their derivatives with respect to the flow direction x, in (1)–(5), can be obtained by solving the two-dimensional ionizing boundary-layer equations. Details of an implicit six-point finite-difference method for solving the two-temperature non-equilibrium boundary-layer equations for ionizing argon were given by Liu and co-workers (1978, 1979). Comparison between the first-order results, without taking into account the mutual interactions between the inviscid and the viscous flows, and the experimental data for both quasi-steady flat-plate and side-wall boundary-layer flows were also given.

In the present study, an iterative scheme for solving (1)–(5) together with the boundary-layer equations was devised. The shock structures, side-wall boundary-layer

flows and the quasi-steady flat-plate boundary-layer flows were re-examined and compared with experiments.

Once the boundary-layer properties and the dissipation terms at the shock-tube sidewall are known, (1)–(5) can be solved for the five unknowns, u, p, T_a, α and T_e, with the following initial conditions:

$$\left.\begin{aligned} \frac{u}{(\gamma RT_0)^{\frac{1}{2}}} &= \frac{(\gamma-1)M_s^2+2}{(\gamma+1)M_s^2}; \\ \frac{p}{p_0} &= \frac{2\gamma M_s^2-\gamma+1}{\gamma+1}; \\ \frac{T_a}{T_0} &= \frac{p}{\rho}\frac{1}{RT_0}; \quad \alpha = 0; \quad \frac{T_e}{T_0} = 1; \end{aligned}\right\} \tag{8}$$

where

$$\frac{\rho}{p_0/RT_0} = \frac{(\gamma+1)M_s^2}{(\gamma-1)M_s^2+2} \quad \text{and} \quad \gamma = \tfrac{5}{3}.$$

The subscript 0 denotes the values before the shock front in shock-fixed co-ordinates.

The computational procedures are as follows: (1) Calculate the (first-order) ionizing shock structure without taking into account flow non-uniformities and wall-dissipation terms. (2) Using these shock-structure results calculate the boundary-layer equations and all boundary-layer thicknesses and dissipation terms. (3) By applying these various boundary-layer results solve the shock-wave structure. (4) Repeat the procedure until the solutions converge to a preset criterion. From our experience, the solutions converge within two or three iteration cycles. A more detailed description of the present analysis is given by Takayama & Liu (1979).

The assumption that the side-wall boundary-layer effects on shock structure can be neglected is only good when

$$\left|\frac{d\delta^*}{dx}\right| \ll \frac{2}{5}\frac{\rho RT_I}{p}\frac{(A-\delta^*L)}{L}\frac{d\alpha}{dx}. \tag{9}$$

This condition can be satisfied only for a shock tube with large cross-sectional area.

In summary, the following differences exist between the present study and the Mirels' analysis: (1) The flow non-uniformities in the momentum and energy equations are included in the present analysis while Mirels (1966) only considered the mass non-uniformity. (2) A similarity assumption was made by Mirels (1963, 1964, 1966) in solving the boundary-layer equations whereas in the present analysis the variations of transport properties were included and the complete boundary-layer equations were solved by a finite-difference scheme.

3. Comparisons between analyses and experiments

The physical models and parameters used in the descriptions of the elastic and inelastic energy-transfer rates, radiation-energy losses, chemical-reaction rates and plasma-transport properties in the present work are the same as those used in previous studies (Glass & Liu 1978; Liu & Glass 1979). Comparisons between analyses and experiments for the shock structures, shock-tube side-wall boundary-layer flows and flat-plate boundary-layer flows are described by the following.

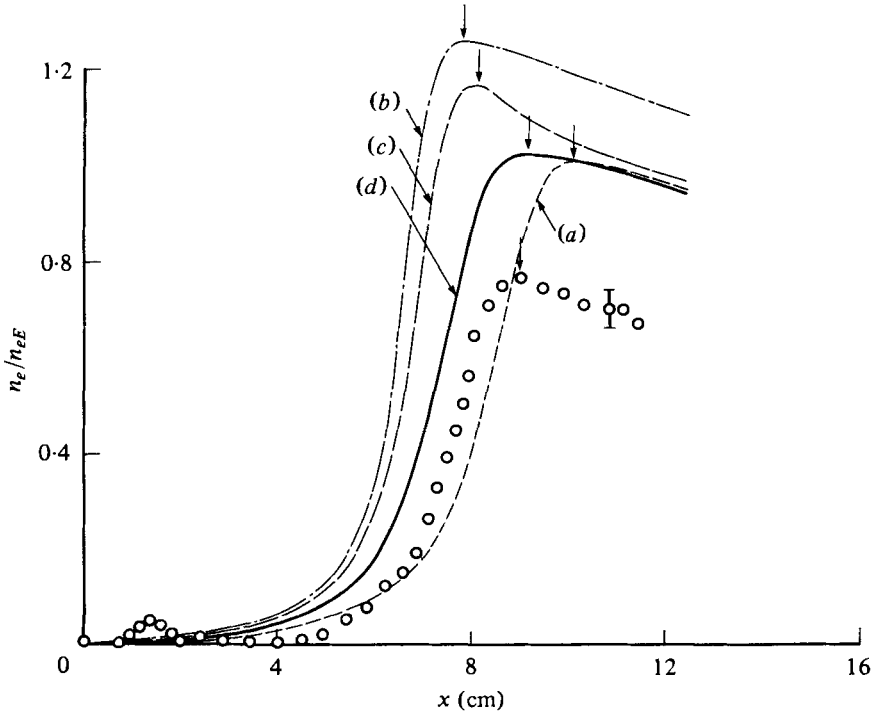

FIGURE 1. Variations of normalized electron number-density n_e/n_{eE} with distance x for case with $M_s = 13{\cdot}1$, $p_0 = 5{\cdot}16$ Torr and $T_0 = 300$ K. Subscript E denotes quasi-equilibrium value. (*a*) First-order results without mutual interactions; (*b*) Enomoto's (1973) model; (*c*) first iterative result of present method; (*d*) final iterative result of present method. Arrow ↓ indicates x_E.

Effects of the side-wall boundary layer on shock structure

In our previous studies of ionizing-argon shock structure, it was shown that the experimental results for higher shock Mach number ($M_s \sim 16$) are in good agreement with the analysis. However, the agreement between analysis and experiment was not as satisfactory for the lower Mach number ($M_s \sim 13$) in comparisons of ionization-relaxation lengths and electron number-density at the electron-cascade front. Two cases ($M_s = 13{\cdot}1$, $p_0 = 5{\cdot}16$ Torr and $M_s = 15{\cdot}9$, $p_0 = 5{\cdot}10$ Torr) which were investigated in previous shock-tube side-wall boundary-layer flows (Liu & Glass 1979) are re-examined in the present analyses.

Figure 1 shows a comparison between the various analyses and the experimental data for the electron number-density profile at the lower-Mach-number case ($M_s = 13{\cdot}1$). Figure 1 (*a*) is the (first-order) result without taking into account the effects of the side-wall boundary layer. Figure 1 (*b*) is the result obtained from Mirels' similar solution of the boundary-layer equations and only considers the nonuniform-flow effect in the mixture mass-conservation equation. It is similar to Enomoto's model. Figure 1 (*c*) is the first iterative result where the boundary-layer equations were solved by an implicit finite-difference scheme and the wall-momentum and energy transfers are taken into account in the inviscid-flow field. Figure 1 (*d*) is the higher-order iterative result. It is seen that the difference between the present model (figure 1 *d*) and

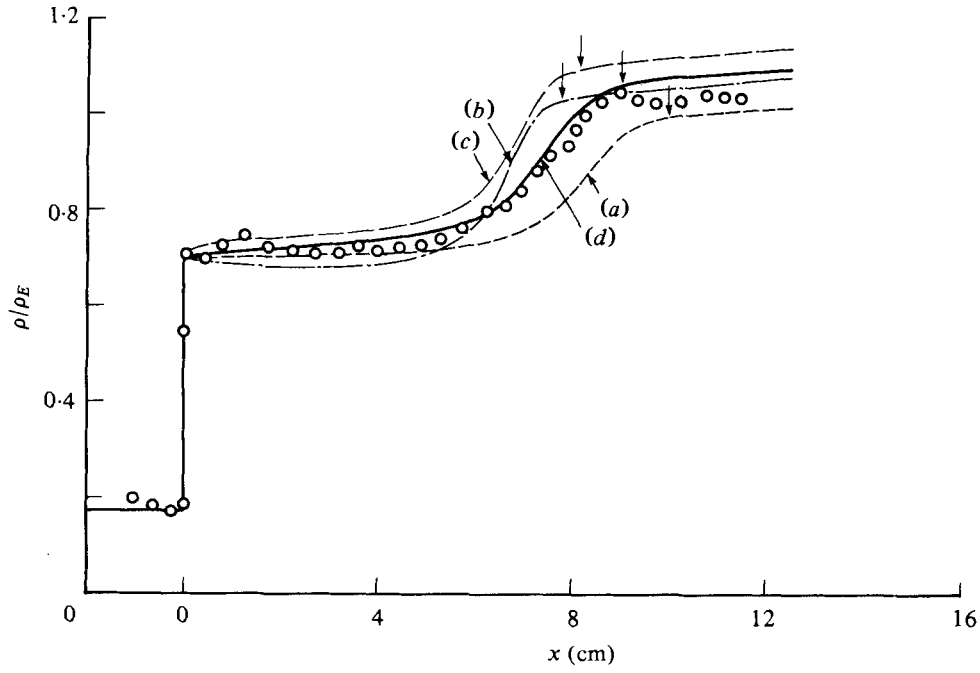

FIGURE 2. Variations of normalized total-plasma-density profiles ρ/ρ_E with distance x for case with $M_s = 13{\cdot}1$, $p_0 = 5{\cdot}16$ Torr and $T_0 = 300$ K. (For other notations see figure 1.)

Enomoto's model (figure 1*b*) is significant for this low-Mach-number case. The electron number-density at the electron-cascade front predicted by using Mirels' method is much higher than that predicted by the present method or by the model without taking into account the mutual interactions. The relaxation length x_E is drastically reduced in Enomoto's model ($x_E = 7{\cdot}8$ cm), while the present method predicts $x_E = 8{\cdot}93$ cm and the corresponding result is about 10 cm for the model without taking into account the mutual interactions. The agreement between the present analysis and experimental data is improved for this low-Mach-number case. It can be explained as follows. In the first-order model without boundary-layer effects, the total-mass flux of the plasma remains constant in the shock-fixed co-ordinates and the quasi-equilibrium peak of the electron number-density profile is reached mainly owing to ionization and recombination processes. However, in the model where the boundary-layer displacement is included, the mass flux is always smaller than that just behind, even though the volumetric flow rate always remains constant. It can be seen from (4) that the quasi-equilibrium peak of electrons or the relaxation length is roughly proportional to the inverse of the mass flux. Therefore, the relaxation length is shortened and the degree of ionization is over-reached in Enomoto's model. However, in the present model where the dissipation terms and other boundary-layer effects are taken into account the relaxation length is larger than that predicted by Enomoto and the overshoot of the degree of ionization is comparatively suppressed.

The corresponding comparison between the analyses and the experimental data for the total plasma density is shown in figure 2. Much better agreement is obtained between the present model and experiment. The relaxation length is reduced by about

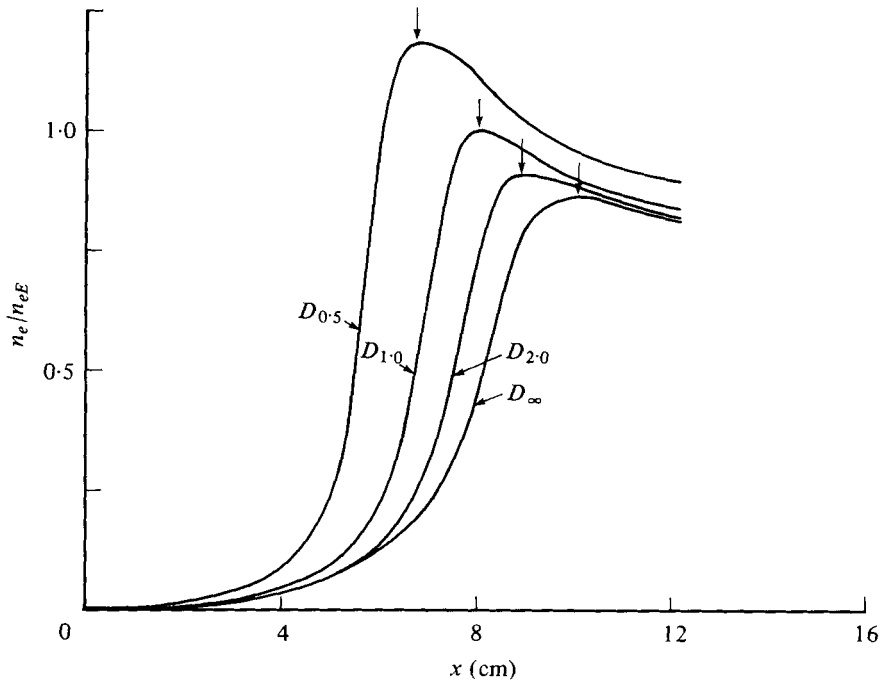

FIGURE 3. Variations of normalized electron number-density profiles n_e/n_{eE} with distance x for various shock-tube hydraulic-diameters D for case with $M_s = 13{\cdot}1$, $p_0 = 5{\cdot}16$ Torr and $T_0 = 300$ K. Curve $D_{0.5}$, $D = 6{\cdot}43$ cm; curve $D_{1.0}$, $D = 12{\cdot}86$ cm (for present tube); curve $D_{2.0}$, $D = 25{\cdot}72$ cm; curve D_∞, $D \to \infty$ cm.

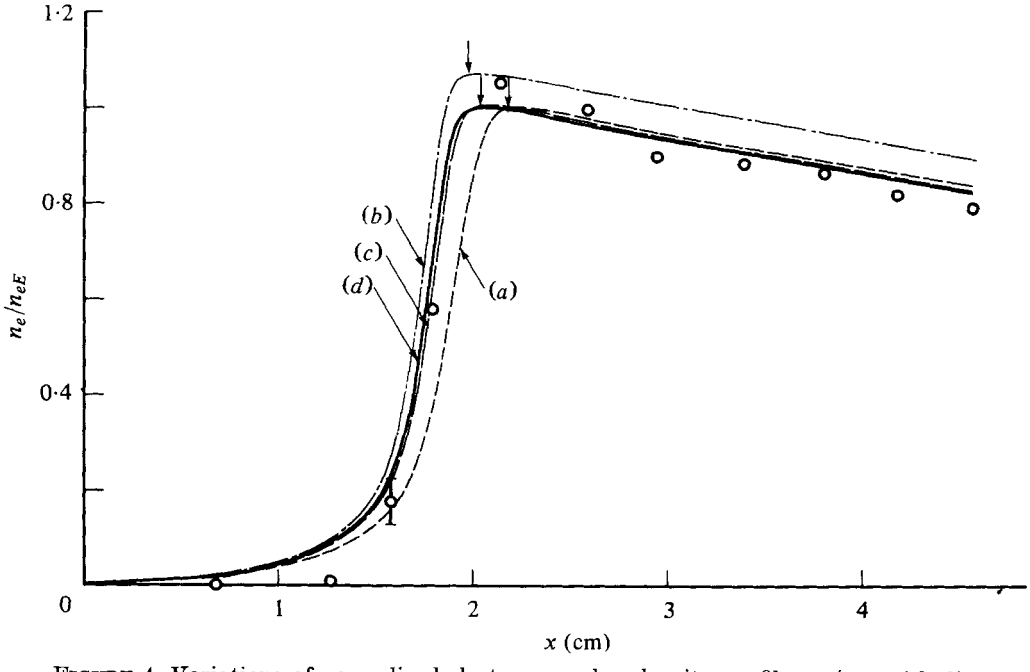

FIGURE 4. Variations of normalized electron number-density profiles n_e/n_{eE} with distance x for case with $M_s = 15{\cdot}9$, $p_0 = 5{\cdot}1$ Torr and $T_0 = 298$ K. (For other notations see figure 1.)

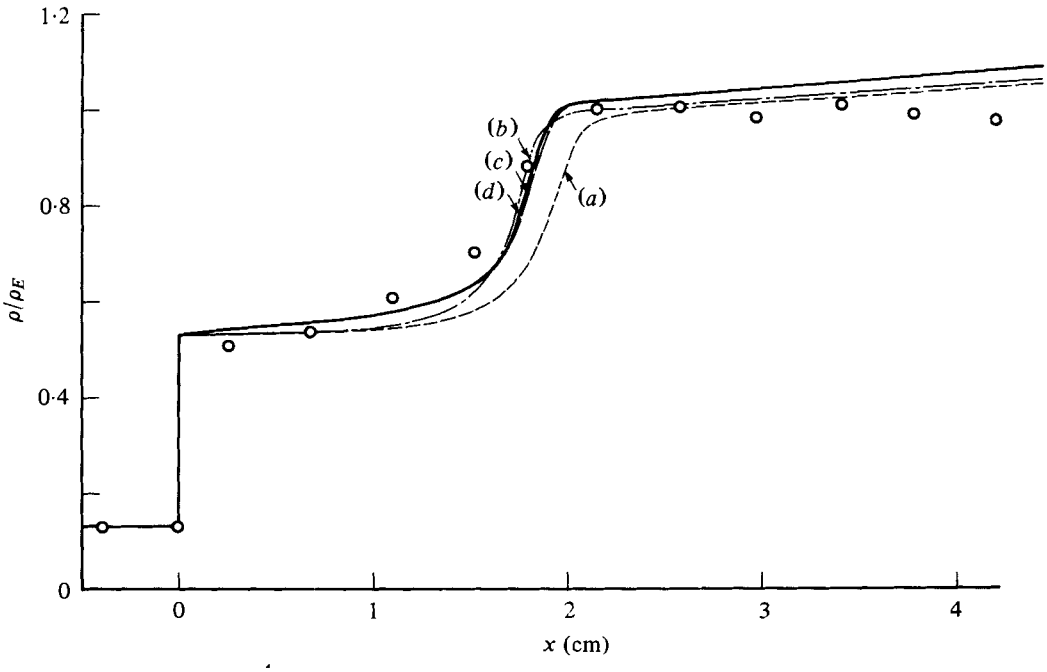

FIGURE 5. Variations of normalized total plasma-density profiles ρ/ρ_E with distance x for case with $M_s = 15{\cdot}9$, $p_0 = 5{\cdot}1$ Torr and $T_0 = 298$ K. (For other notations see figure 1.)

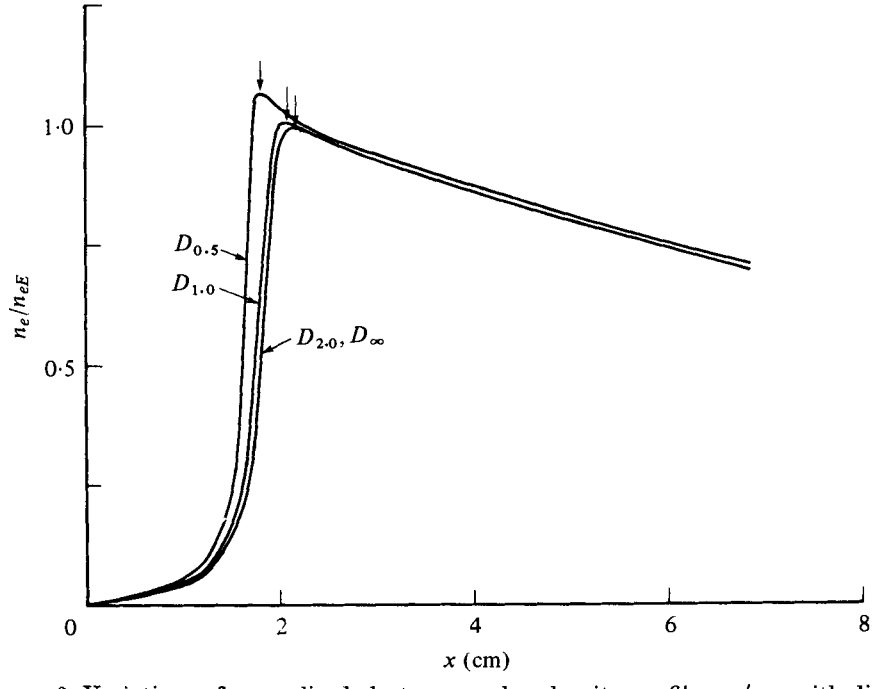

FIGURE 6. Variations of normalized electron number-density profiles n_e/n_{eE} with distance x for various shock-tube hydraulic-diameter D for case with $M_s = 15{\cdot}9$, $p_0 = 5{\cdot}1$ Torr and $T_0 = 298$ K. (For other notations see figure 3.)

12 % owing to the side-wall boundary-layer growth for this low-Mach-number case. Details of the boundary-layer-thickness profiles (δ's) are given by Takayama & Liu (1979).

In order to investigate the shock-tube-diameter effects on shock structure, different shock-tube diameters were used in the calculations. Figure 3 shows the results for the electron number-density profile with various shock-tube hydraulic-diameters. It is seen that the relaxation lengths decrease and the electron number-density at the cascade front increases as the shock-tube diameter decreases. Consequently, the smaller the shock-tube diameter, the more pronounced are the effects of the side-wall boundary layer.

In the second case at higher shock Mach number, $M_s = 15{\cdot}9$, the experimental and analytical results for the electron number-density profiles are shown in figure 4. In this case, the difference between the present model (figure 4*d*) and Enomoto's model (figure 4*b*) is much smaller than in the previous low-Mach-number case. The reason is that the effects of the boundary-layer dissipation terms and the effects of the momentum and energy non-uniformities due to the side-wall boundary-layer growth on shock structure are small since the relaxation length is much shorter at high Mach number. Much better agreement is obtained by using the present model for the plasma-density profile shown in figure 5 in the initial ionization region. The effects of shock-tube diameter on shock structure are shown in figure 6. It is seen that the effects of shock-tube diameter on shock-wave structure is much smaller for stronger shock waves since the relaxation length is much shorter and the dwell time for boundary-layer effects is reduced. The relaxation length is shortened only by 6 % owing to the side-wall boundary-layer effects at the higher Mach number.

From the previous comparisons between analyses and experimental data the following can be concluded. (1) The previously-determined value of the argon–argon collisional cross-section constant of $1{\cdot}0 \times 10^{-19}$ eV cm^{-2} (see Glass & Liu 1978) is accurate. (2) Relaxation lengths are reduced significantly in shock tubes of finite area owing to the side-wall boundary-layer growth at lower shock Mach numbers when the relaxation lengths are large. The same conclusion was made by Enomoto and his pioneering analysis was very worth while. (3) The model suggested by Enomoto which neglected the momentum and energy non-uniformities and the dissipation terms in the inviscid flow field over-predicts the effects of boundary-layer growth on shock structure for low-Mach-number cases. Therefore, the application of Mirels' method to ionizing-gas flows is not appropriate, except to obtain a rough estimate of the effects of the side-wall boundary layer on shock structure. (4) The effects of side-wall boundary layer on shock structure are more pronounced for small diameter shock tubes. For the large 10×18 cm UTIAS Hypervelocity Shock Tube these effects are reduced and the results approach one-dimensional values.

Shock-tube side-wall boundary-layer flows

Shock-tube side-wall boundary-layer flows in ionizing argon without taking into account the mutual interactions between the inviscid and the viscous flows were analysed and compared with dual-wavelength interferometric data by Liu & Glass (1979). Satisfactory agreement was obtained for the low-shock-Mach-number case, $M_s = 13{\cdot}1$. The experimental results lie between the frozen and non-equilibrium

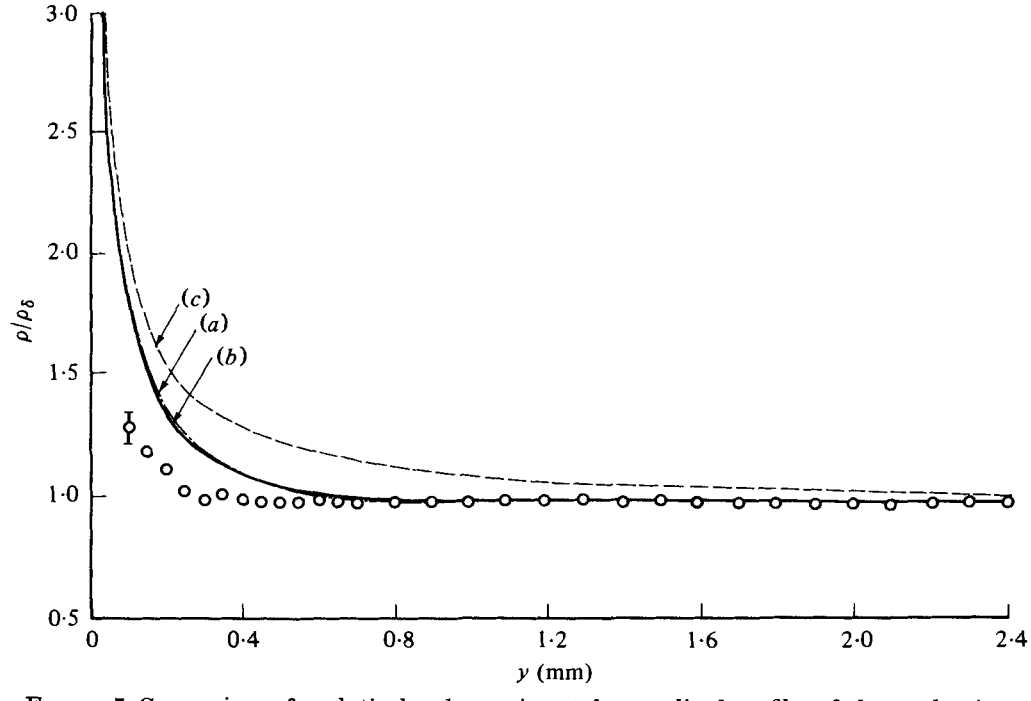

FIGURE 7. Comparison of analytical and experimental normalized profiles of plasma density ρ/ρ_δ with distance y in the side-wall boundary layer in argon at $x = 9{\cdot}5$ cm, $M_s = 13{\cdot}1$, $p_0 = 5{\cdot}16$ Torr and $T_0 = 300$ K. (*a*) First-order result; (*b*) present result; (*c*), frozen solution.

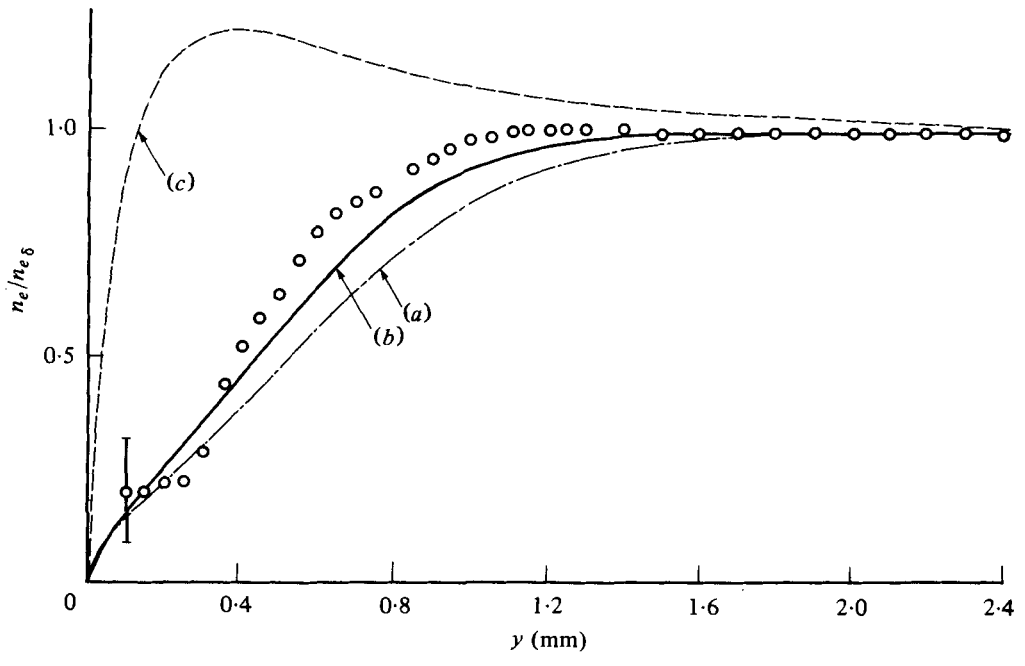

FIGURE 8. Comparison of analytical and experimental normalized electron number-density profiles $n_e/n_{e\delta}$ with distance y in the side-wall boundary layer in argon at $x = 9{\cdot}5$ cm, $M_s = 13{\cdot}1$, $p_0 = 5{\cdot}16$ Torr and $T_0 = 300$ K. (For other notations see figure 7.)

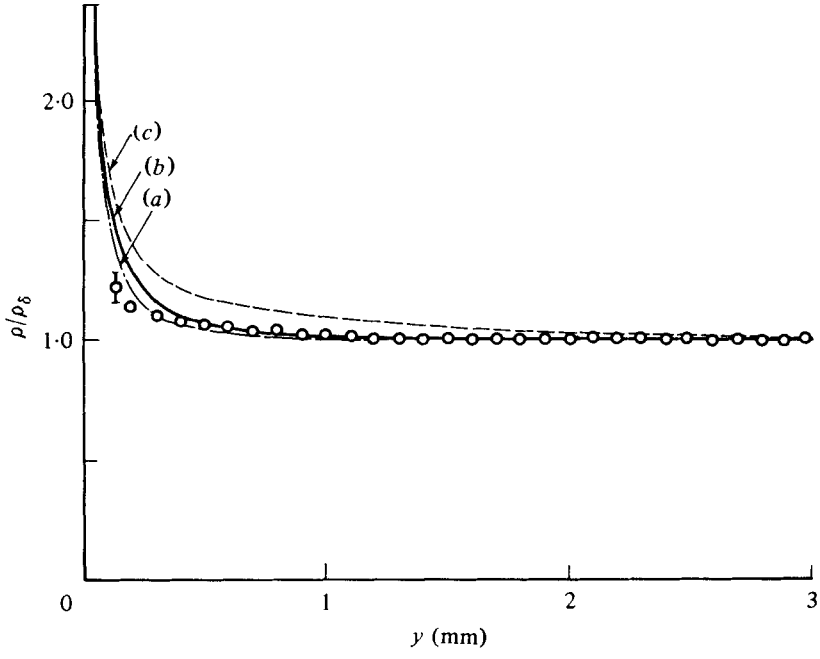

FIGURE 9. Comparison of analytical and experimental normalized profile of plasma density ρ/ρ_δ with distance y in the side-wall boundary layer at $x = 18$ cm, $M_s = 15{\cdot}9$, $p_0 = 5{\cdot}1$ Torr and $T_0 = 298$ K. (For other notations see figure 7.)

solutions. However, it was found that two-dimensional effects were significant for the higher-Mach-number case, $M_s = 15{\cdot}9$. The phenomenon of the electron-cascade front moving in toward the wall to approach the translational shock wave was found more prominent for stronger shock waves (Glass & Liu 1978). Some reasons for this premature ionization and relaxation process are given in Takayama & Liu (1979).

The present side-wall boundary-layer results were obtained by using the shock-structure solutions described previously as the edge conditions of the boundary layer. The difference between the previous model (Liu & Glass 1979) without taking into account the mutual interactions and the present results arises from the changes in the free-stream-flow properties. As expected, changes in the free-stream-flow conditions will cause changes in the boundary-layer flows.

Figure 7 shows the corresponding first-order and present results for the case of $M_s = 13{\cdot}1$ and $p_0 = 5{\cdot}16$ Torr together with the experimental data for the plasma-density profiles. The difference between the first-order and the present coupled results is small since it has been shown before (Liu *et al.* 1978; Liu & Glass 1979) that the total plasma-density profile is not a sensitive indicator of boundary-layer structure. However, the difference between the first-order and the present results for the electron number-density profiles can be readily seen in figure 8, even though the difference is not large. It is evident that the present results agree better with the experimental data than the first-order results for the lower-Mach-number case, where the premature ionization and recombination effects close to the wall are not significant in the experiments (Glass & Liu 1978).

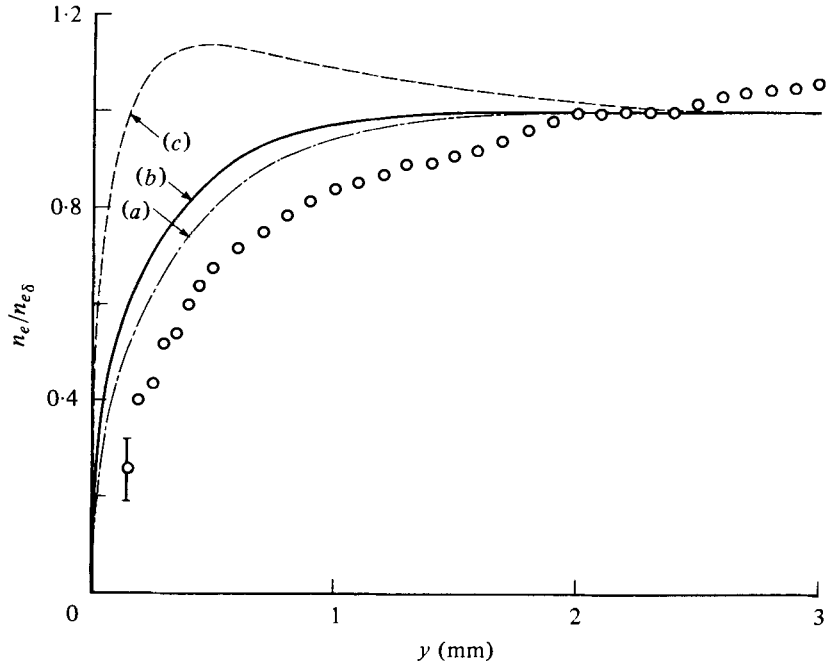

FIGURE 10. Comparison of analytical and experimental normalized profiles of electron number-density $n_e/n_{e\delta}$ with distance y in the side-wall boundary layer at $x = 18$ cm, $M_s = 15{\cdot}9$, $p_0 = 5{\cdot}1$ Torr and $T_0 = 298$ K. (For other notations see figure 7.)

For the higher-Mach-number case, $M_s = 15{\cdot}9$ and $p_0 = 5{\cdot}1$ torr, the analytical results are shown in figures 9 and 10 for the plasma density and electron number-density, respectively. It is found that the agreement with the experimental data is worse for the present results. The reason for the discrepancies between these two causes are as follows. It was shown (Glass & Liu 1978) that coupled sinusoidal disturbances occur at high shock Mach numbers in the translational-shock front and in the electron-cascade front and in the flow beyond. Recently, the flow profiles in a direction normal to the wall were measured in the inviscid flow region. It was found that the flow was non-uniform in the inviscid region at this high Mach number. In the experiment, the electron number-density kept on increasing with distance from the wall and did not reach an asymptotic value at $y = 14$ mm. The total plasma density decreased from the wall and reached its asymptotic value at the edge of the boundary layer. However, it decreased again when the distance from the wall was greater than 8 mm. This flow non-uniformity behind a moving shock wave at higher Mach number arises mainly from a radiation-energy transfer. Such two-dimensional effects on shock structure cannot be predicted by employing quasi-one-dimensional models as used in the previous and present analyses. Improvements could be obtained by utilizing time-dependent two-dimensional models in order to understand the flow non-uniformities induced by radiation-energy transfer.

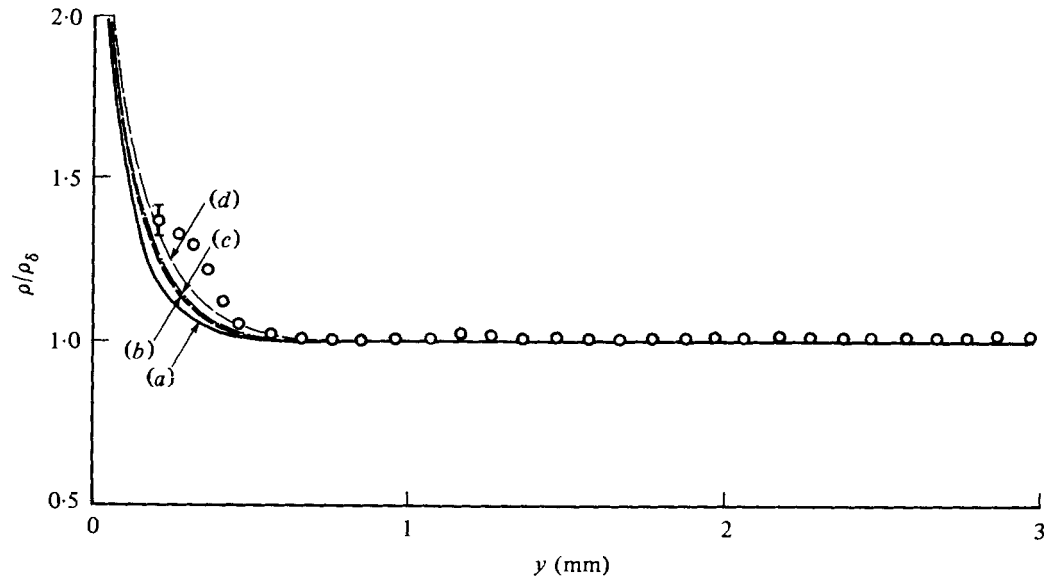

FIGURE 11. Comparison of analytical and experimental normalized profiles of plasma density ρ/ρ_δ with distance y in the flat-plate boundary layer at $x = 14$ cm, $M_s = 16{\cdot}6$, $p_0 = 4{\cdot}81$ Torr and $T_0 = 296$ K. (*a*) Present non-equilibrium; (*b*) present frozen; (*c*) first-order non-equilibrium; (*d*) first-order frozen.

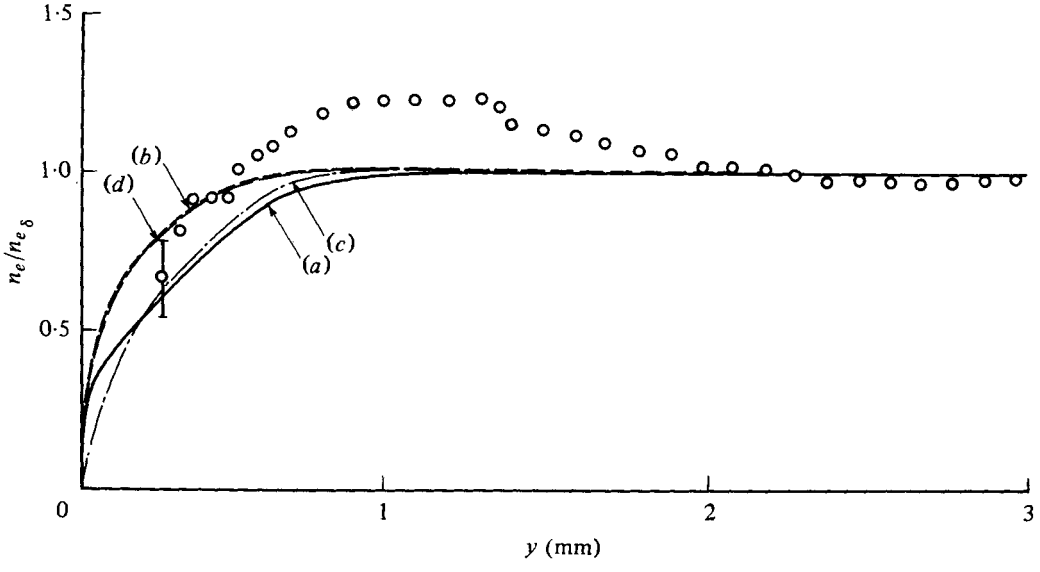

FIGURE 12. Comparison of analytical and experimental normalized electron number-density profile $n_e/n_{e\delta}$ with distance y in the flat-plate boundary layer. (Initial conditions and notations are given in figure 11.)

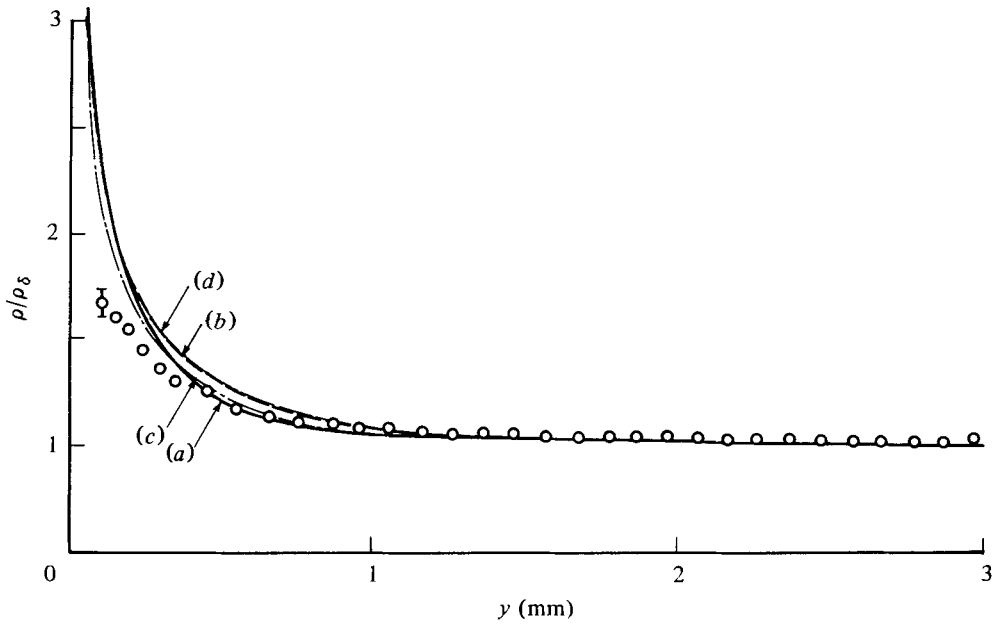

FIGURE 13. Comparison of analytical and experimental normalized profile for plasma density ρ/ρ_δ in the flat-plate boundary layer at $x = 14$ cm, $M_s = 12{\cdot}8$, $p_0 = 5{\cdot}01$ Torr and $T_0 = 297$ K. (For other notations see figure 11.)

Quasi-steady flat-plate boundary-layer flows

The first-order results of the quasi-steady flat-plate boundary-layer flows generated by a strong shock wave in a shock tube in ionizing argon were given and compared with dual-wavelength interferometric data by Liu *et al.* (1978). Satisfactory agreement was obtained between analysis and experimental plasma-density and electron number-density profiles for cases $M_s \sim 13$ and 16.

Two cases reported previously, $M_s = 12{\cdot}8$, $p_0 = 5{\cdot}01$ torr and $M_s = 16{\cdot}6$, $p_0 = 4{\cdot}81$ torr, were re-analysed using the present method. The difference between the previous results (Liu *et al.* 1978) and the present analysis arises from the change in the free-stream-flow conditions resulting from the mutual interactions between the inviscid and viscous flows.

Figure 11 shows comparisons between analyses and the experimental data for the plasma density profile with $M_s = 16{\cdot}6$ and $p_0 = 4{\cdot}81$ torr. The difference is quite small between the first-order result, without taking into account the mutual interactions, and the present analysis. The corresponding results for the electron number-density profile is plotted in figure 12. A bump appearing in the experimental data for the electron number-density profile was not significant in the present analysis. The disagreement between theory and experiment for n_e mainly results from the fact that the boundary-layer flow is assumed to be quasi-steady while in the experiments it is unsteady owing to radiation-energy losses. The variations of the flow properties with distance x have not been taken into account in the flat-plate case in order to satisfy the steady-state condition.

For the second case $M_s = 12{\cdot}8$ and $p_0 = 5{\cdot}01$ torr, the non-equilibrium and frozen-

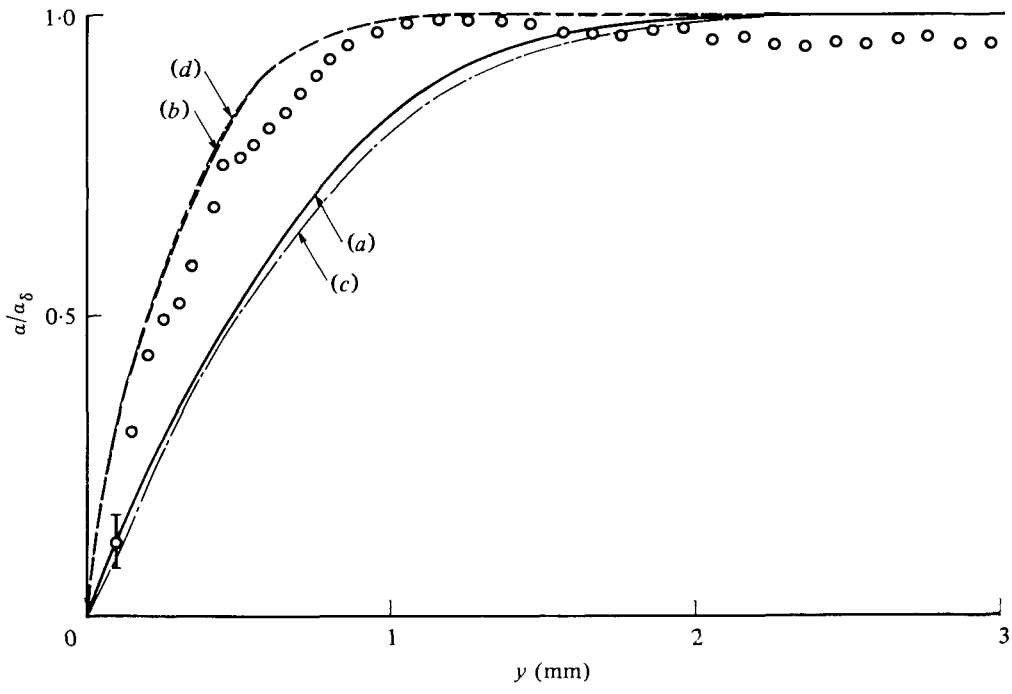

FIGURE 14. Comparison of analytical and experimental normalized profile for electron number-density $n_e/_{e\delta}$ in the flat-plate boundary layer at $x = 14$ cm, $M_s = 12{\cdot}8$, $p_0 = 5{\cdot}01$ torr and $T_0 = 297$ K. (For other notation see figure 11.)

flow profiles for plasma density and for electron number-density are shown in figures 13 and 14, respectively, together with the experimental data. A small improvement is found by using the present method. The experimental results for n_e lie between the analytical non-equilibrium and frozen-flow profiles.

It has been shown that the effects of the mutual interactions between the inviscid free-stream and the viscous side-wall boundary layer on the flat-plate boundary-layer flows generated in a shock tube are small. Unsteady effects are dominant for flat-plate boundary-layer flows generated by strong shock waves in a shock tube at high shock Mach numbers owing to radiation effects.

4. Discussion and conclusions

The second-order terms, $\partial(\mu\,\partial u/\partial x)/\partial x$ and $\partial(\lambda\,\partial T/\partial x)/\partial x$, arising from the plasma bulk viscosity and the thermal conduction were neglected in the analysis owing to the very small velocity and temperature gradients along the flow direction in the relaxation region. Near the electron-cascade front, the second-order terms have the same order of magnitude as the wall-dissipation terms. However, the effects of the second-order terms on the required relaxation length are small. The length where the second-order terms cannot be neglected is about 10 % of the total relaxation length.

The unsteady effects on shock-wave structure were shown to be of a minor nature in the experiments (Glass *et al.* 1977; Glass & Liu 1978). However, two-dimensional effects on the side-wall boundary-layer flow were shown to be significant in the high

shock-Mach-number experiment. The order of magnitude of the two-dimensional effect is not easy to estimate except through a difficult unsteady two-dimensional analysis. This is a major limitation of the present analysis. Presently, the unsteady effects on the flat-plate boundary-layer flow generated in the shock tube cannot be evaluated without a two-dimensional analysis of the shock-wave structure.

Within the foregoing limitations it can be concluded that the present analysis of the mutual-in teraction effects of ionizing-argon shock-structure and shock-tube side-wall boundary-layer flows is based on the most reasonable physical model now available. The effective quasi-one-dimensional shock-structure equations for a tube of finite area are derived from a flow area-average concept. The flow non-uniformities resulting from the boundary-layer-displacement thickness and other defined thicknesses as well as wall dissipation are included in the shock-structure analysis. The results are compared with a previous first-order analysis and interferometric data at nominal shock Mach numbers of 13 and 16 at an initial pressure of 5 torr. It is shown that a perfect-gas analysis based only on displacement thickness overestimates the reduction in shock-structure thickness. However, a real-gas analysis shows that the actual shock-structure thickness is closer to the idealized one-dimensional case for shock tubes of reasonable cross-sections, such as the UTIAS 10×18 cm Hypervelocity Shock Tube. In addition, our interferometric measurements of the electron number-density and total-density shock-structure profiles as well as the derived degree of ionization profiles are in much better agreement with the present analysis than those we reported previously. The same remarks apply to the ionizing boundary-layer interferometric profiles. The agreement of our experimental data with the present analysis is very good for both the shock structure and the boundary layer at $M_s \sim 13$ and at $M_s \sim 16$. For further details see Takayama & Liu (1979).

A further investigation based on the time-dependent Navier–Stokes equations may be required in order to predict the two-dimensional effects on shock structure and the unsteady effects on induced flat-plate boundary-layer flows, which are not included in the present study.

The financial assistance received from the National Research Council of Canada and the U.S. Air Force Office of Scientific Research under Grant no. AF-AFOSR-77-3303 are acknowledged with thanks.

REFERENCES

BRABBS, T. A. & BELLES, F. E. 1971 In *Proc. 8th Int. Shock Tube Symp.* (ed. S. L. Stollery, A. G. Gaydon & P. R. Owen), p. 24/1. London: Chapman & Hall.

ENOMOTO, Y. 1973 *J. Phys. Soc. Japan* **35**, 1228.

GLASS, I. I., LIU, W. S. & TANG, F. C. 1977 *Can. J. Phys.* **56**, 1269.

GLASS, I. I. & LIU, W. S. 1978 *J. Fluid Mech.* **84**, 55.

GLASS, I. I. & PATTERSON, G. N. 1955 *J. Aero. Sci.* **22**, 73.

HUBBARD, E. W. & DE BOER, P. C. T. 1969 In *Proc. 7th Int. Shock Tube Symp.* (ed. I. I. Glass), p. 109. University of Toronto Press.

KAMIMOTO, G., TESHIMA, K. & NISHIMURA, M. 1972 *Kyoto University Rep.* C.P. 36.

LIU, W. S. & GLASS, I. I. 1979 *J. Fluid Mech.* **91**, 679.

LIU, W. S., WHITTEN, B. T. & GLASS, I. I. 1978 *J. Fluid Mech.* **87**, 609.

MCLAREN, T. I. & HOBSON, R. M. 1968 *Phys. Fluids* **9**, 2162.

MIRELS, H. 1963 *Phys. Fluids* **6**, 1201.

MIRELS, H. 1964 *A.I.A.A. J.* **2**, 84.
MIRELS, H. 1966 *Phys. Fluids* **9**, 1907.
TAKAYAMA, K. & LIU, W. S. 1979 *UTIAS Rep.* no. 233.
TRIMPI, R. L. & COHEN, N. B. 1955 *N.A.C.A. Tech. Note* TN 3375.